

Robust Weight Imprinting: Insights from Neural Collapse and Proxy-Based Aggregation

Justus Westerhoff

DATEXIS, Berliner Hochschule für Technik (BHT), Germany

justus.westerhoff@bht-berlin.de

Golzar Atefi

DATEXIS, Berliner Hochschule für Technik (BHT), Germany

Mario Koddenbrock

KI Werkstatt, Hochschule für Technik und Wirtschaft Berlin (HTW), Germany

Alexei Figueroa

DATEXIS, Berliner Hochschule für Technik (BHT), Germany

Alexander Löser

DATEXIS, Berliner Hochschule für Technik (BHT), Germany

Erik Rodner

KI Werkstatt, Hochschule für Technik und Wirtschaft Berlin (HTW) & Merantix Momentum, Germany

Felix A. Gers

DATEXIS, Berliner Hochschule für Technik (BHT), Germany

Reviewed on OpenReview: <https://openreview.net/forum?id=duU11BnQ3Y>

Abstract

The capacity of foundation models allows for their application to new, unseen tasks. The adaptation to such tasks is called transfer learning. An efficient transfer learning method that circumvents parameter optimization is imprinting. The conceptual differences between studies on imprinting form the basis of our systematic investigation. In this work, we propose the general IMPRINT framework, identifying three main components: generation, normalization, and aggregation. Through the lens of this framework, we conduct an in-depth analysis and a comparison of the existing methods. Our findings reveal the benefits of representing novel data with multiple proxies in the generation step and show the importance of proper normalization. Beyond an extensive analytical grounding, our framework enables us to propose a novel variant of imprinting which outperforms previous work on transfer learning tasks by 4%. This variant determines proxies through clustering motivated by the neural collapse phenomenon – a connection that we draw for the first time. We publicly release our code at <https://github.com/DATEXIS/IMPRINT>.

1 Introduction

In machine learning applications, training models from scratch is often not viable due to limitations in data and compute. A popular solution is to apply transfer learning (Bengio, 2012; Yosinski et al., 2014) based on foundation models (FMs) (Bommasani et al., 2021) that are pre-trained on a large amount of data. To tune a FM to a novel task, e.g., for classification, a common procedure is to freeze the model parameters and replace the output layer with a new head. A particularly simple method for implementing such a new head was proposed by Qi et al. (2018) and coined *imprinting*.

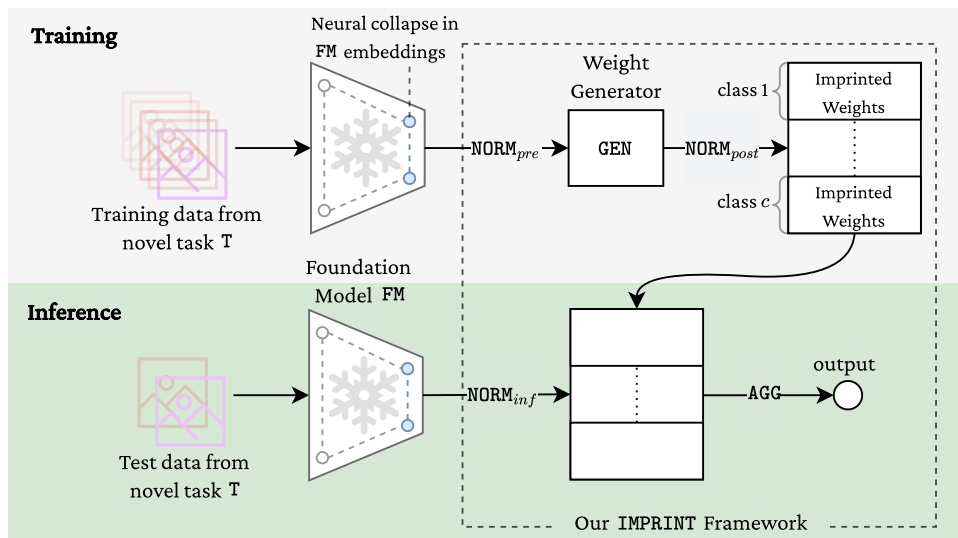


Figure 1: Overview of our IMPRINT framework. The foundation model FM is frozen and shows neural collapse. The weight generator (GEN) uses training data from a novel task T to consecutively generate one or more weight vectors (proxies) per class $1, \dots, C$ in T . In inference, the final output for the test data in T is computed by an aggregation (AGG) mechanism. Embeddings and generated weights are normalized according to $NORM_{pre}$ and $NORM_{post}$, respectively. During inference, embeddings are normalized according to $NORM_{inf}$.

Imprinting. In the original work by Qi et al. (2018), the last-layer weight vector of a novel class is set to the normalized average of its scaled embedding vectors, i.e., its class mean. These class means are representatives of the classes, which we denote as *proxies*. In general, we refer to imprinting as efficient learning methods without the need for cross-class statistics or gradient-based optimization. A plethora of studies have emerged surveying this technique by adding complexity and adaptability (Gidaris & Komodakis, 2018; Siam et al., 2019; Passalis et al., 2020; Khan et al., 2021; Li et al., 2021; Cristovao et al., 2022; Yan et al., 2023). Despite its many adaptations, imprinting lacks a systematic comparison that unifies them. Understanding its variations could unlock greater efficiency across many fields, making the method even more versatile and impactful.

Applications. In particular, while in some practical applications, accuracy is prioritized over computational efficiency, the latter does become a critical requirement in scenarios where computational resources are severely constrained, e.g., in the chemical and polymer processing industries. Here, battery-powered edge compute is essential and frequent retraining or large-scale optimization is infeasible. Imprinting has proven particularly effective in these contexts of edge-embedded devices (Passalis et al., 2020). For instance, Zhu et al. (2022) implement a vision-based robotic force grasping with a variable-stiffness gripper that can safely handle both fragile and heavy objects by rapidly adapting to novel categories without retraining (Continual Learning (CL) setting). Industrial adoption also underscores this trend with Google’s Coral Edge TPU including an `ImprintingEngine` API (Coral), that allows users to add new classes from a few examples without recompiling the model. Very recently, (Belal et al., 2025) apply imprinting to spectrogram embeddings from IMU/EMG gait data, achieving efficient classification in low-data Human Activity Recognition (HAR) tasks. Apart from that, Janson et al. (2022) extend imprinting to CL, establishing a simple baseline with competitive performance compared to more sophisticated state-of-the-art CL algorithms.

Framework. We present IMPRINT, a framework that enables a comprehensive analysis of existing imprinting techniques. More precisely, we generalize prior work by decomposing imprinting into three principal steps (see fig. 1). During generation (GEN) of weights, the method selects representative data samples and generates one or more weight vectors (proxies) per class. Normalization (NORM) is crucial, as the generated weights need to be balanced. Aggregation (AGG) entails the computation of the final output, e.g., a class label. The computational efficiency of imprinting allows us to perform a large number of experiments. Through IMPRINT, we are able to propose a novel, best-performing imprinting strategy using multi-proxy weight imprinting in combination with L^2 normalization, outperforming previously studied methods, as depicted in fig. 2.

Neural Collapse. When neural networks are trained to reach near-zero loss, their penultimate-layer embeddings collapse to the class means (Papayan et al., 2020; Zhu et al., 2021). We investigate this phenomenon as a potential explanation for when and why imprinting works. Our analysis proves that there exists a relationship between a measure of neural collapse and the success of imprinting. Since quantification of this phenomenon is possible in a post-hoc fashion over the FM features, we believe that these insights will contribute to further development of imprinting methods, as well as, training regimes of FMs that are more suitable for transfer learning via imprinting.

Contributions. In summary, our main results and contributions are:

- We deconstruct weight imprinting into the IMPRINT framework composed of generation, normalization, and aggregation, and discuss variations for each of them, while identifying prior work as special cases (section 3.1). To the best of our knowledge, we are the first to conduct a comprehensive analysis of imprinting to this scale (section 4).
- We present a new, outperforming imprinting method utilizing k -means clustering for weight generation (section 5.1) and show its benefits in certain low-data regimes (section 5.2).
- As far as we are aware, we are the first to identify a relationship between the degree of neural collapse and imprinting success (section 5.3).

2 Related Work

Imprinting and Low-Data Regimes. Weight imprinting is implemented by setting the final layer weights for the novel classes to the scaled average of the embedding vectors of their training samples and was first introduced by Qi et al. (2018) for the few-shot learning scenario. The authors find that for up to 20 samples, using a combination of imprinting and fine-tuning outperforms other state-of-the-art methods, including nearest neighbor algorithms. In contrast, in our work we do not limit the number of samples and perform no fine-tuning on the imprinted weights to maintain efficiency.

Imprinting has been applied to object detection (Li et al., 2021; Yan et al., 2023), multi-label classification (Khan et al., 2021), semantic segmentation (Siam et al., 2019), and combined with an attention mechanism to generate weights for the novel classes in a few-shot classification task (Gidaris & Komodakis, 2018).

Hosoda et al. (2024) apply imprinting using quantile normalization to ensure statistical similarity between new and existing weights. We consider this as one normalization scheme in our framework. Zhang et al. (2021) apply imprinting in chest radiography for detection of COVID-19 and find that it yields better results than joint gradient descent training of all classes when only few samples are available. They speculate whether normalization is a constraint in their imprinting model.

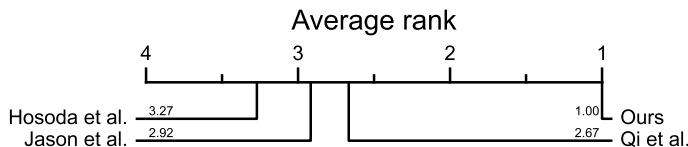
Before the era of deep learning, Mensink et al. (2013) analyze the transferability of hand-crafted image features. They use a “nearest class multiple centroids” (NMC) classifier with multiple proxies generated from a k -means clustering algorithm. In combination with metric learning, they compare favorably against the m -nearest neighbor algorithm. Our work, on the other hand, highlights efficient transfer learning provided by foundation models.

Transfer Learning. Using embedding vectors from pre-trained models is a simple and widely used transfer learning approach, established in the seminal works on computer vision (Donahue et al., 2014) and natural language processing (Devlin et al., 2019). Kornblith et al. (2019) show that pre-training performance of a model is highly correlated with the performance of the resulting embedding vectors in downstream tasks. In addition, Huh et al. (2016) provide insights into the required quality of pre-training data. Our work is orthogonal to these studies, since we focus on studying weight generation, normalization, and aggregation techniques applied later on for new task adaptation.

Continual Learning (CL). Although we investigate transfer learning scenarios, we review the imprinting applications and results from CL. Rebuffi et al. (2017) dynamically select a subset of examples for each class and update internal representations via gradient descent. They use a nearest mean classifier (NMC)

Table 1 & Figure 2: Previously studied imprinting strategies are special cases within IMPRINT. We evaluate 12 different classification tasks T s derived from *MNIST*, *FashionMNIST*, and *CIFAR-10*, each with 10 classes or subsets thereof, and 4 pre-trained models FM s (*resnet18*, *resnet50*, *vit_b_16*, *swin_b*). The proposed configuration (“Ours”) derived from IMPRINT outperforms previous work across FM s and T s by a large margin with statistical significance, as confirmed by the critical difference (CD) diagram below. Since absolute accuracies vary substantially across tasks and models (as reflected by the large standard deviations (std)), this rank-based aggregation is used for fair comparison. Here, $k = 20$ is used, highlighting the gain of using multiple proxies per class. For reference, the gray row reports an oracle method that uses cross-class feature statistics to generate weights (see appendix A.5). It is not an imprinting method and therefore not directly comparable to the imprinting-based approaches above. Nonetheless, the results indicate that our method substantially narrows the gap between single-proxy mean imprinting and this oracle baseline.

Work	$NORM_{pre}$	GEN	$NORM_{post}$	$NORM_{inf}$	AGG	Avg. acc. % \pm std
Qi et al. (2018)	L2	mean	L2	L2	max	86.79 \pm 7.83
Hosoda et al. (2024)	none	mean	quantile	none	max	82.90 \pm 12.87
Janson et al. (2022)	none	mean	none	none	1- <i>nn</i>	86.64 \pm 7.88
Ours	L2	k-means	L2	L2	max	91.06 \pm 6.21
Oracle	none	least-squares	none	none	max	94.54 \pm 5.00



with respect to the saved examples. Janson et al. (2022) use an NMC classifier as well and achieve good performance on CL benchmarks without any fine-tuning of the embeddings. However, they do not investigate the effect of normalization and using multiple proxies.

Findings of Prabhu et al. (2023) show that a simple, approximate m -nearest neighbor classifier outperforms existing methods in an Online CL setting when all data can be stored. In our work, however, we compare imprinting all data to a limited number of more representative proxies striving for efficiency.

Neural Collapse (NC). The phenomenon of NC was identified by Pappayan et al. (2020) and refers to the convergence of the last-layer weight vectors to class means. It was shown that, regardless of the loss function, optimizer, batch-normalization, or regularization, NC will eventually occur (provided the training data has a balanced distribution) (Zhu et al., 2021; Han et al., 2022; Kothapalli, 2023). Nevertheless, complete neural collapse is practically unrealistic (Tirer et al., 2023). In transfer learning, Galanti et al. (2022) show that NC occurs on new samples and classes from the same distribution as the pre-training dataset, highlighting the usability of foundational models in such scenarios. In our work, we expand the survey on NC by experimenting with out-of-distribution classes belonging to different datasets and linking their degree of collapse to the success of certain imprinting strategies.

3 Methods

3.1 IMPRINT

In order to find out how to best and efficiently set the classifier weights of a foundational model FM in new, previously unseen tasks T , we create the IMPRINT framework (see fig. 1) that generalizes previous work, specifically all the methods that work without access to cross-class statistics and gradient-based training. Thereby, we unify all the existing imprinting strategies described in section 2.

Overview. We analyze the effect of weight generation (**GEN**), normalizations (**NORM** = $\{\text{NORM}_{pre}, \text{NORM}_{post}, \text{NORM}_{inf}\}$), and aggregation (**AGG**). The **IMPRINT** framework depicted in fig. 1 consists of three main building blocks: a foundation model **FM**, a weight generator **GEN**, and extendable classifier weights that are imprinted. The **FM** remains frozen throughout the experiments. It receives data from **T** as inputs and produces embedding vectors. The training process generates weight vectors for each of the C classes in **T**. Hereby, embeddings from the **FM** are normalized before the generation (**GEN**) step according to NORM_{pre} . The generated weight vectors per class are referred to as *proxies*, prototypes, or representatives (Movshovitz-Attias et al., 2017; Snell et al., 2017; Yang et al., 2018; Yu et al., 2020). These proxies are normalized according to NORM_{post} . As in the work by Qi et al. (2018), we do not use bias values. To classify the test data in **T** during inference, it is first embedded by the **FM**, normalized according to NORM_{inf} , and finally aggregated by **AGG**, resulting in a predicted class label.

Generalization of Previous Methods. Previously proposed imprinting methods can be defined as special cases of our framework. We design **IMPRINT** such that every method can be defined by a single combination of **GEN**, **NORM**, and **AGG**, of which we inspect all possible combinations.

Weight Generation (GEN). The purpose of **GEN** is to determine how the embeddings of the training data in **T** are used to form the new weights. In contrast to Qi et al. (2018) which only incorporates one proxy per class (the mean), we add flexibility by allowing each class to have multiple proxies as in Mensink et al. (2013) and enable non-linear classification. We denote the number of proxies per class as k , ranging between 1 and the number of samples, and investigate the following operations **conducted per class** to generate those:

- **all**: All embeddings (denoted as $k = \text{all}$).
- **k-random**: k random embeddings.
- **mean**: The mean of all embeddings.
- **k-means**: k -means cluster centers using **KMeans** from *sklearn* (Pedregosa et al., 2011). $k = 1$ is the same as **mean**.
- **k-medoids**: k -medoids cluster centers using **KMedoids** from *sklearn*.
- **k-cov-max** (covariance-maximization): Top k embeddings by covariance (in code: `proxies = embeddings[torch.argsort(torch.sum(torch.cov(embeddings), dim=0), descending=True)[:k]]`).
- **k-fps** (farthest-point sampling): Iteratively selecting k embeddings, such that it maximizes the distance from already selected ones (starting with a random sample).

We choose this diverse list of methods to cover a wide range of approaches, ranging from heuristics (e.g., **k-fps**) to more complex algorithms (e.g., **k-means**). Note that only **mean** and **k-means** generate proxies beyond existing samples by producing synthetic cluster centers in embedding space. In comparison, **k-medoids** must choose actual samples as cluster centers (analogous to a median). None of these methods use cross-class statistics or gradient-based optimization. We also note an analogy to associative memory models, interpreting imprinting as a memory update process following a covariance rule, as detailed in appendix A.3.

Normalization (NORM). The main reason for applying normalization is to allow each embedding and weight vector to contribute equally on the same scale. The modes we allow are no normalization (**none**), L^2 normalization (**L2**), and quantile normalization (**quantile**).

L2 normalization can be applied to embeddings before **GEN** via NORM_{pre} , to the generated weights via NORM_{post} , and to embeddings in inference via NORM_{inf} . In any case, the vector is L^2 -normalized by dividing it by its Euclidean length $\|\cdot\|_2$.

quantile normalization (Amaratunga & Cabrera, 2001; Bolstad et al., 2003) can only be applied to generated weights. This non-linear operation distributes weights equally. Recall that if more than one class is contained in **T** ($c > 1$), **GEN** is performed for each class consecutively, and the reference distribution changes accordingly. In particular, for the first class there is no reference distribution to map to. This is different from Hosoda et al. (2024), where new weights are matched to the distribution of the original classifier weights of the **FM**.

Since we do not consider the classes used for pre-training the FM and especially do not assume access to their last-layer weights, this is not possible in our scenario.

Aggregation (AGG). There are various ways to use the generated weights (proxies) per class during inference, especially when $k > 1$. We focus on two different modes, **max** and m -nearest neighbor (**m-nn**). The former, **max**, computes the inner product of the input embedding and the imprinted weights and outputs the class label with the maximum activation. The latter, **m-nn**, uses the class weights as keys and the embeddings as values, and chooses the final winning output class via the m -nearest neighbor algorithm. The **m-nn** voting is weighted by the inverse of the Euclidean distances to their nearest neighbor, turning it into weighted majority voting.

We also experimented with alternative distance functions (Cosine, Manhattan) and uniform weighting, but found differences well within statistical noise. Using the Mahalanobis distance proved computationally prohibitive. More elaborate voting mechanisms, such as learned top- k attention or entropy-based filtering, are conceivable, but extend well beyond the minimalist imprinting paradigm and therefore left for future work.

Note that **max** is the same as **1-nn** in the case of L2 for $NORM_{post}$, since for any fixed embedding vector \mathbf{v} and variable proxy \mathbf{w} , the argmin of $\|\mathbf{v} - \mathbf{w}\|^2 = \|\mathbf{v}\|^2 - 2\langle \mathbf{v}, \mathbf{w} \rangle + \|\mathbf{w}\|^2$, calculated by **1-nn**, is the same as the argmax of the inner product $\langle \mathbf{v}, \mathbf{w} \rangle$ calculated in **max**.

3.2 Quantifying Neural Collapse

Neural collapse (NC) (Papayan et al., 2020) characterizes the state of the features produced by a classification neural network after training to near zero training loss. Namely, the learned embeddings of each class converge, i.e., *collapse*, to their class means. These globally centered class means and classifier weights form a simplex equiangular tight frame (ETF) – a collection of equal length and maximally equiangular vectors, that maximize the between-class variability. This results in an optimal linearly separable state for classification. In fig. 3 (left), we illustrate the collapse of a FM on its pre-training data. The newly arrived data T from a different dataset is distributed more unevenly across the embedding space (right).

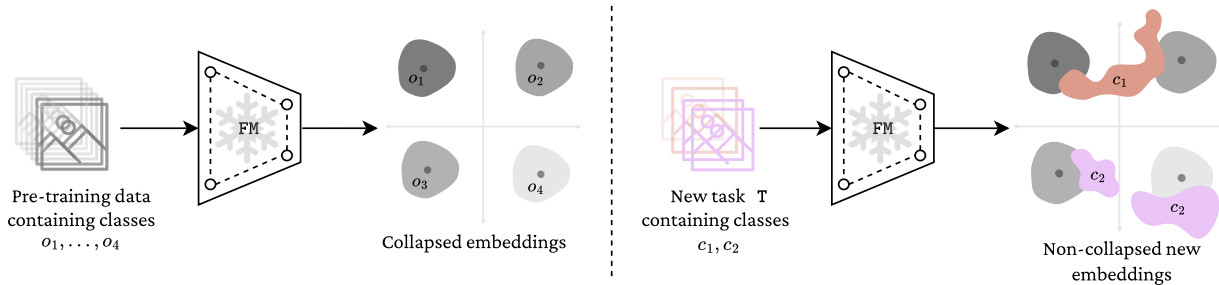


Figure 3: Left: The embeddings of the pre-training data, after being used to train the foundation model FM, show neural collapse, as each class (o_1, \dots, o_4) is evenly separated in space and accumulates around their respective class means. Right: For a novel task with classes c_1, c_2 (pink and brown) scatter around the collapsed pre-trained classes (gray).

Two important characteristics of NC are **variability collapse**, i.e., the within-class variability of the penultimate-layer embeddings collapses to zero, and **convergence to nearest-mean-classification**. We focus on variability collapse (\mathcal{NC}_1) as in Zhu et al. (2021). Given a foundation model FM and a finite dataset containing C classes with (for simplicity) N samples per class, we use its l -dimensional embeddings $\{\mathbf{h}_{c,i}\}_{1 \leq c \leq C, 1 \leq i \leq N}$ given by FM to define the global feature mean $\mathbf{h}_G := \frac{1}{CN} \sum_{c=1}^C \sum_{i=1}^N \mathbf{h}_{c,i}$, class means $\bar{\mathbf{h}}_c := \frac{1}{N} \sum_{i=1}^N \mathbf{h}_{c,i}$, the within-class covariance matrix $\Sigma_W := \frac{1}{CN} \sum_{c=1}^C \sum_{i=1}^N (\mathbf{h}_{c,i} - \bar{\mathbf{h}}_c)(\mathbf{h}_{c,i} - \bar{\mathbf{h}}_c)^\top$, and the between-class covariance matrix $\Sigma_B := \frac{1}{C} \sum_{c=1}^C (\bar{\mathbf{h}}_c - \mathbf{h}_G)(\bar{\mathbf{h}}_c - \mathbf{h}_G)^\top$ to finally compute

$$\mathcal{NC}_1 = \frac{1}{C} \text{trace}(\Sigma_W \Sigma_B^+), \tag{1}$$

where $^+$ symbolizes the pseudo-inverse.

Based on eq. (1), an \mathcal{NC}_1 score closer to zero signifies a higher collapse. In contrast, an increase in modality of data leads to a higher \mathcal{NC}_1 score (as analyzed in fig. 11a). Note that this measurement is not independent of the embedding dimension l and the number of classes C . According to NC, imprinting the mean, as originally done by Qi et al. (2018), is best when \mathcal{NC}_1 is small. We claim that when the data is not fully collapsed (as is often the case in practice), the scale of \mathcal{NC}_1 could guide the proxy generation method, e.g., having multiple proxies $k > 1$ per class. We investigate this in section 5.3.

3.3 Significance Testing with Critical Difference Diagrams

Our experiments compare large numbers of imprinting configurations across tasks with substantially different achievable accuracy levels. To obtain scale-independent statistical comparisons, we base our analysis on ranking (dis-)agreements rather than raw accuracy. Non-parametric rank-based tests are well suited for this setting. Following Demšar (2006), we use the Friedman test and Wilcoxon signed-rank tests because they do not assume normality or homoscedasticity, and can be applied uniformly to any evaluation metric. Empirical evidence in Demšar (2006) further suggests that these tests have good power in classifier comparison scenarios.

Concretely, for each evaluation instance (i.e., foundation model **FM** and task **T**) we compute the classification accuracy of all configurations and assign ranks (rank 1 = highest accuracy). This yields a matrix of ranks with one row per configuration and one column per evaluation instance. On this matrix we first apply the Friedman test to assess whether there are any overall differences between configurations. If the Friedman test rejects the global null hypothesis at significance level $\alpha = 0.05$, we proceed with a post-hoc, pairwise analysis. Specifically, for every pair of configurations we run a two-sided Wilcoxon signed-rank test across evaluation instances. The resulting p -values are corrected for multiple comparisons using the Holm step-down procedure (Holm, 1979).

Critical difference (CD) diagrams summarize both the average performance and the significance structure. The horizontal axis shows the average rank of each configuration across all evaluation instances, with lower ranks indicating better performance. Two configurations are connected by a thick horizontal line if their Wilcoxon–Holm comparison does not show a significant difference.

4 Experimental Setup

Foundation Models FM. We use `resnet18`, `resnet50` (He et al., 2016), `vit_b_16` (Dosovitskiy et al., 2021), and `swin_b` (Liu et al., 2021) as **FMs**, two CNN-based and two Transformer-based architectures. All four models are pre-trained on *ImageNet-1K* (ILSVRC 2012) (Deng et al., 2009). To generate the embeddings, we use PyTorch’s *torchvision* models.

Tasks T. We analyze multi-class classification scenarios without separating base and new classes, instead focusing on all classes within a novel **T** at the same time. To investigate the effect of the number of samples given, we look at **n-shot** ($n \in \mathbb{N}$) scenarios. For that, we randomly pre-sample the training data of **T** to n samples per class – transitioning into the low-data regime.

To find out the best imprinting strategy within our **IMPRINT** framework, we focus on tasks **T** created from the datasets *MNIST* (Deng, 2012), *FashionMNIST* (Xiao et al., 2017), and *CIFAR-10* (Krizhevsky et al., 2009), each containing 10 classes. We mainly focus on the three **T** containing all ten classes. Furthermore, we look at smaller tasks only containing classes $\{0, 1, 2\}$, and the two tasks containing classes $\{1, 3, 5, 7, 9\}$ resp. $\{0, 2, 4, 6, 8\}$. This random selection of $3 \cdot 4 = 12$ tasks adds variation to our evaluations.

Neural Collapse. In the analysis of neural collapse (NC), we also look at the **FMs**’ pre-training data (*ImageNet*). As its test set is not available, we use its validation set in \mathcal{NC}_1 computations. Furthermore, for *ImageNet*, we relabel data by combining multiple classes into one label to simulate multi-modal class distributions for an in-depth NC analysis. These tasks are called “ d in 1”, $d = 1, \dots, 10$, each containing 10 different labels. More precisely, we take 100 random classes from *ImageNet* and sequentially map the first d to label 1, the second d to label 2, etc., until we reach 10 distinct labels. See fig. 4 for a simplified illustration.

Moreover, we construct a new out-of-distribution, non-collapsed dataset by merging all classes from four digit datasets: *MNIST*, *MNIST-M* (Ganin et al., 2016), *SVHN* (Netzer et al., 2011), and *USPS* (Hull, 1994). The resulting dataset, which we refer to as *CombiDigits*, exhibits reduced collapse due to the greater distributional diversity within each class. To ensure scale invariance in covariance-based NC measurements, all embeddings are L^2 -normalized before computing \mathcal{NC}_1 .

Scale. In total, we ran approximately 500 000 experiments, varying imprinting components, foundation models, tasks, and seeds. This is feasible with minimal effort as imprinting is a highly efficient method: core steps such as weight generation (GEN), normalization (NORM), and aggregation (AGG) are linear in dataset size or number of proxies and parallelize efficiently within each step. Details on experimental infrastructure and parallelization are provided in appendix A.6.

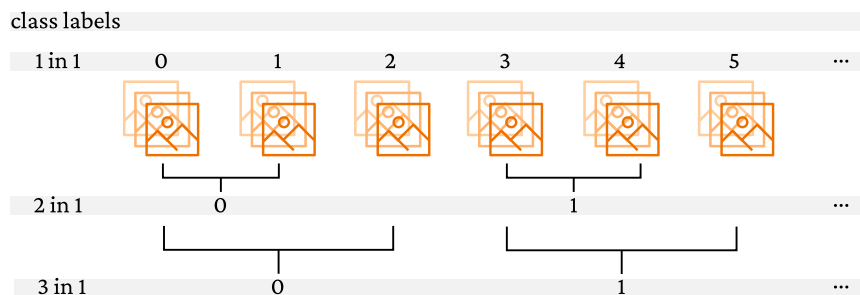


Figure 4: Combining multiple classes into one to create tasks with multi-modal class distributions. Simplified example for “ d in 1”, $d = 1, 2, 3$, with only six (instead of 100) original classes.

Evaluation. Unless stated otherwise, we report the median test accuracy over three different seeds. In sections 5.1 and 5.2, we evaluate the imprinting performance by varying the FM (4) and T (12) and report average accuracy and standard deviation (std) across these. Due to the heterogeneity of models and tasks, large std are expected. Therefore, overall method comparisons are based on ranks rather than absolute accuracies. Methods are ranked by their median accuracy, yielding $4 \cdot 12 = 48$ potentially different ranks. We report the average rank and assess statistical significance of ranking (dis-)agreements using critical difference (CD) diagrams as explained in section 3.3. The code used to generate these diagrams is inspired by Ismail Fawaz et al. (2019).

In experiments with neural collapse (section 5.3), we investigate the four FMs on 100 random *ImageNet* tasks with remapped labels (as explained above) and the four tasks containing all of *MNIST*, *FashionMNIST*, *CIFAR-10*, and *CombiDigits*, respectively.

5 Results

Our main experimental insights are: **1.** Our IMPRINT framework generalizes previous methods, and we find a new superior imprinting strategy (section 5.1). **2.** We show that our novel strategy is even beneficial in low-data regimes with as little as 50 samples per class (section 5.2). **3.** We identify a correlation between imprinting success utilizing multiple proxies and a measure of neural collapse (section 5.3).

5.1 Best Imprinting Strategy

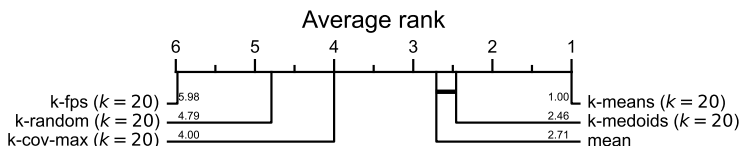
We provide a comparison between existing memory-constrained methods used for imprinting on foundation models in fig. 2, namely, the work by Qi et al. (2018); Hosoda et al. (2024); Janson et al. (2022), as well as a novel, best-performing configuration (“Ours”) that results from IMPRINT. Focusing on $k = 20$, we find that our method, consisting of k -means weight generation, L2 normalizations, and \max aggregation, outperforms all previously studied approaches by a margin of 4% on average with statistical significance. For reference, we additionally report an oracle baseline that uses cross-class feature statistics to generate its

weights, representing an upper bound that is not constrained by imprinting. The results indicate that our new imprinting method significantly narrows the gap between single-proxy **mean** imprinting and this oracle baseline.

The impact of using the unconstrained **m-nn** aggregation on **all** data is investigated at the end of this section. Next, we analyze each of the components of **IMPRINT** separately.

Table 2 & Figure 5: Benchmarking **GEN** mechanism for $k \leq 20$ across FMs and Ts. Best **NORM** combination for each row used implicitly. **AGG** is fixed to **max**. CD diagram proves that **k-means** weight generation is significantly better than all other methods.

GEN	k	Avg. acc. % \pm std
k-means	20	91.04 ± 6.26
k-medoids	20	87.01 ± 8.23
mean	1	86.84 ± 7.80
k-cov-max	20	83.98 ± 9.56
k-random	20	82.14 ± 10.15
k-fps	20	65.56 ± 12.32



Weight Generation (GEN). To assess the impact of **GEN**, we first focus on the **max** aggregation and do not fix **NORM**, but simply show the run with the best **NORM** combination, if not otherwise specified. The **m-nn** aggregation and different values for **NORM** are analyzed later in this section.

Initially, we limit the number of generated proxies to $k \leq 20$. Results in fig. 5 show how **k-means**, using as many proxies as possible (in this case, 20) outperforms by 4% on average accuracy compared to all the other **GEN** methods. The CD diagram illustrates its statistical significance in ranking. Furthermore, while **k-medoids** with 20 proxies (which necessarily have to be among the given samples, see section 3.1) is computationally expensive, it is on par with **mean**, and covariance maximization, furthest-point sampling and random selection show even weaker performances. We find similar results for $k \leq 5$, where **k-means** outperforms the other methods as well (see fig. A.1).

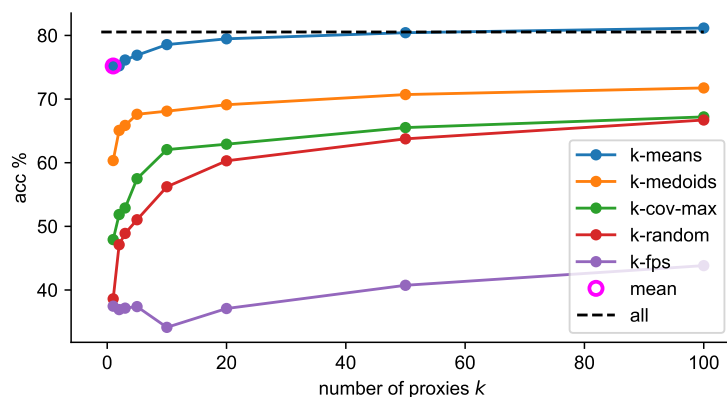


Figure 6: Benchmarking different **GEN** methods with **resnet18** on all of *CIFAR-10* shows superiority of **k-means** proxies. All combinations employ **L2** for all **NORM** and **max** as **AGG**.

As the number of proxies k increases, **k-means** continues to be the best **GEN** method. An example for **resnet18** and *CIFAR-10* can be found in fig. 6. All methods converge towards the point of imprinting (saving) **all** data ($k = \text{all}$), even surpassing it in the case of **k-means**. Due to its superior performance, we mainly focus on **k-means** in the remainder of the analysis.

Learned Weights. Employing gradient-based methods – such as setting weights via the analytical least-squares initialization proposed by Harun & Kanan (2025), which uses data *and labels* from all classes *jointly*

– can be seen as an upper bound (“Oracle” in fig. 2) for the unsupervised weight imprinting approaches discussed here. We extend this method by combining it with **k-means**, forming **k-least-squares**, and observe in appendix A.5 that using multiple proxies per class instead of a single weight vector can still improve performance, particularly on datasets with high \mathcal{NC}_1 .

Normalization (NORM). We compare all the different NORM methods, focusing on **k-means** as **GEN**. For $k = 1$ and varying NORM_{post} (while taking best values for NORM_{pre} and NORM_{inf} implicitly), fig. 7 shows that L2 is the best choice for weight normalization. **quantile** and **none** normalization both perform worse.

Table 3 & Figure 7: Benchmarking NORM_{post} mechanism across FMs and Ts. The best NORM_{pre} and NORM_{inf} combinations for each row are used implicitly. **GEN** is fixed to **mean** (that is, $k = 1$) and **AGG** is fixed to **max**. The CD diagram shows the statistical significance of L2 as the best weight normalization NORM_{post} .

NORM_{post}	Avg. acc. % \pm std
L2	86.84 ± 7.80
quantile	82.90 ± 12.87
none	83.26 ± 9.18

Table 4: Benchmarking NORM_{pre} and NORM_{inf} mechanisms across FMs and Ts. NORM_{post} is fixed to L2, **GEN** to **mean**, and **AGG** to **max**. No statistically significant differences were found.

NORM_{pre}	NORM_{inf}	Avg. acc. % \pm std
none	L2	86.84 ± 7.80
none	none	86.84 ± 7.80
L2	L2	86.79 ± 7.83

Keeping L2 for NORM_{post} fixed, we find no statistical differences between the different combinations of NORM_{pre} and NORM_{inf} (see table 4). For larger values of k , the differences among NORM_{post} become even more pronounced. However, the performance of NORM_{pre} and NORM_{inf} remains statistically indifferent for L2 weight normalization (see fig. A.2 for all combinations at once with $k = 1$, and fig. A.3 for $k = 20$).

We restrict all the subsequent experiments to using L2 across all NORM following Qi et al. (2018). This combination of normalizations is chosen to specifically model cosine similarity within **max** aggregation.

Table 5 & Figure 8: Benchmarking **AGG** mechanism across FMs and Ts. **GEN** is fixed to **all** ($k = \text{all}$), that is, imprinting (saving) all data to weights. L2 normalization is used for all NORM. The CD diagram shows statistical significance of **3-nn**, **5-nn**, and **20-nn** over **max** aggregation.

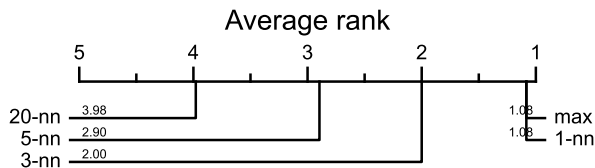
AGG	Avg. acc. % \pm std
5-nn	93.74 ± 4.97
3-nn	93.50 ± 5.22
20-nn	93.56 ± 4.93
1-nn	92.81 ± 5.69
max	92.81 ± 5.69
50-nn	92.91 ± 5.25

Aggregation (AGG). In addition to **max**, we study the effect of using m -nearest neighbor (**m-nn**) as an aggregation method. Recall that **max** is a special case of **m-nn** when $m = 1$ (as NORM_{post} is set to L2). We investigate different values for $m \in \{1, 3, 5, 20, 50\}$.

When **all** data is imprinted, fig. 8 shows that using **m-nn** aggregation for $m \in \{3, 5, 20\}$ is slightly better than **max**. With $k = 20$ and **k-means** as **GEN**, **max** (=1-nn) aggregation becomes the top performing combination

Table 6 & Figure 9: Benchmarking AGG mechanism across FMs and Ts. GEN is fixed to **k-means** with $k = 20$. L2 normalization is used for all NORM. The CD diagram shows that **max** is the best-performing aggregation method.

AGG	Avg. acc. % \pm std
1-nn	91.06 ± 6.21
max	91.06 ± 6.21
3-nn	90.59 ± 6.16
5-nn	90.12 ± 6.21
20-nn	87.05 ± 7.46



(see fig. 9). Furthermore, the reduction of proxies (from **all** (≈ 6000 per class) to $k = 20$) leads to a decrease in accuracy of less than 3%.

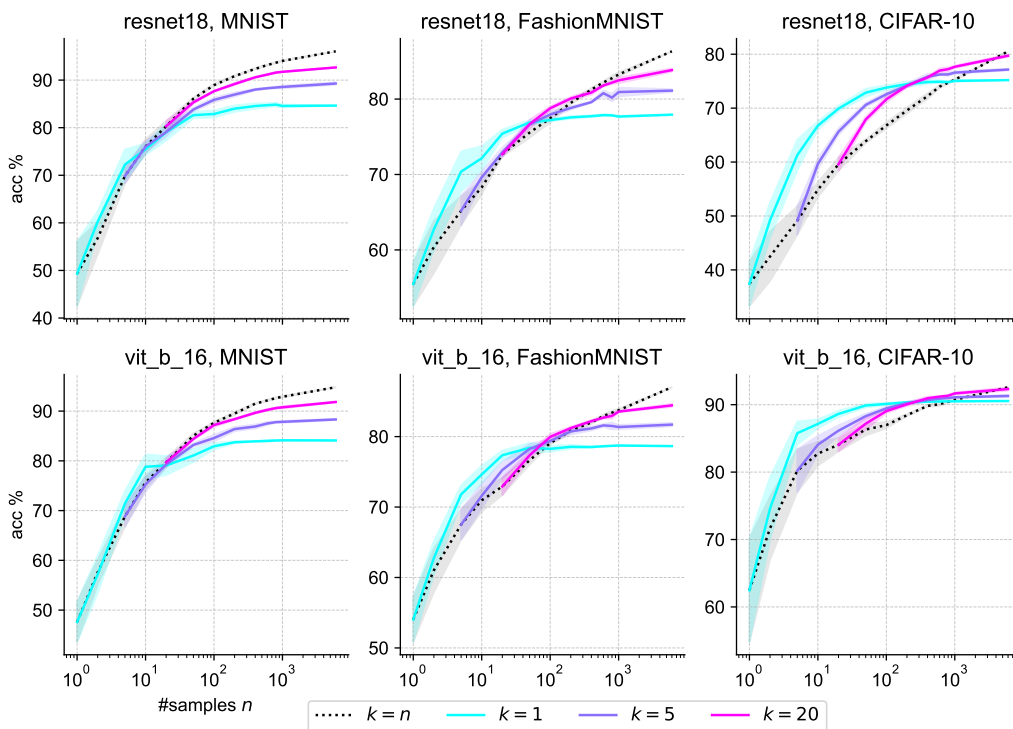


Figure 10: **k-means** with different values for k in **n-shot** scenarios. Shaded areas indicate 95% confidence intervals (CIs) over five different seeds. Other variables are fixed to our previously described best method of using L2 normalizations and **max** as AGG. Note that only data for the meaningful case of $k \leq n$ is shown. For *MNIST* and *FashionMNIST*, **mean** ceases to be the best strategy already at only roughly 50 samples.

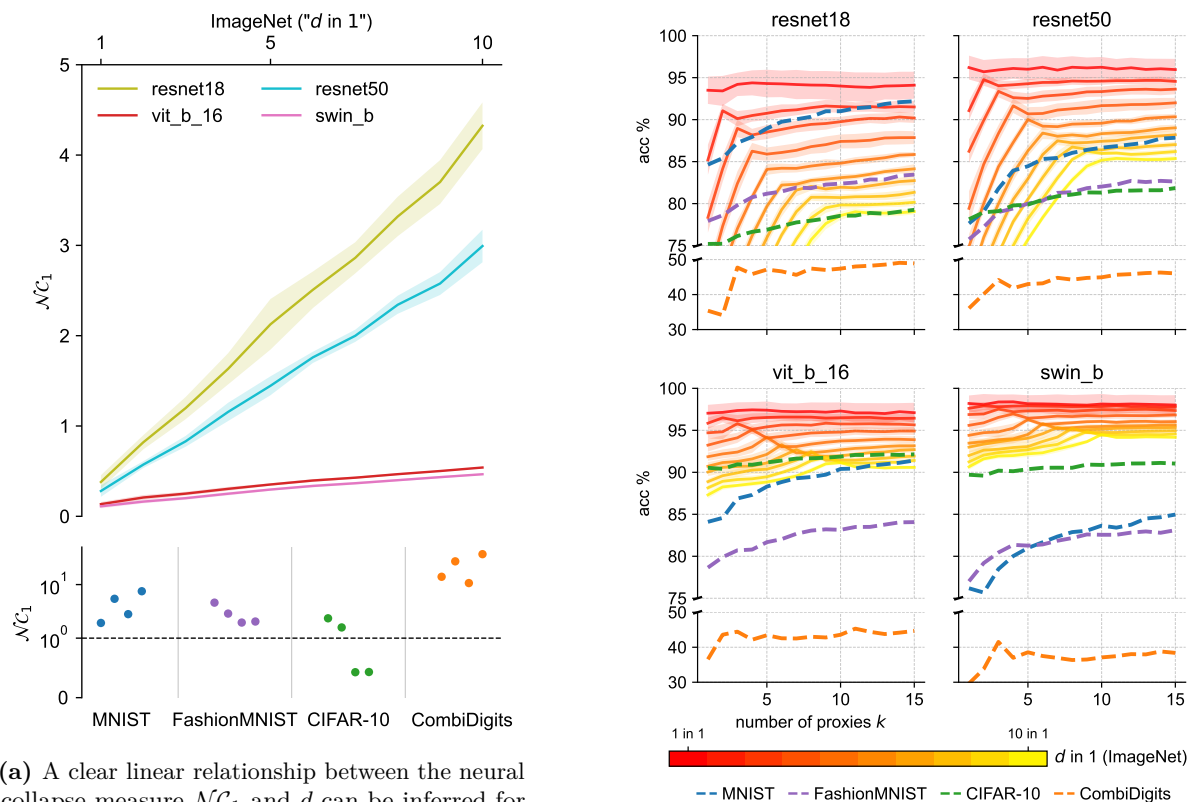
5.2 Low-Data Regime

We analyze the **n-shot** scenario with our method (**k-means** as GEN, L2 as NORM, and **max** as AGG). Furthermore, we focus on the large tasks **T** containing all ten classes of *MNIST*, *FashionMNIST*, resp. *CIFAR-10* at once. In this scenario, due to sampling only a few examples n , we average over five (instead of three) different seeds.

From the results in fig. 10, we find that as the number of samples n increases, **k-means** starts to outperform **mean** imprinting. The use of more proxies k further amplifies this performance gain. The shift occurs at roughly 50 samples per class for *MNIST* and *FashionMNIST*, while for *CIFAR-10*, $k > 1$ becomes prominently better at around 200 samples per class (see fig. A.4 for a display of all FMs focused on $10 \leq n \leq 400$).

5.3 Neural Collapse and Number of Proxies

Figure 11a depicts the neural collapse measurement $\mathcal{N}\mathcal{C}_1$ (see eq. (1)) for the 100 random *ImageNet* tasks with remapped labels as explained in section 4, as well as the four tasks containing all of *MNIST*, *FashionMNIST*, *CIFAR-10*, resp. *CombiDigits*. It can be inferred that *ImageNet* has a close-to-zero $\mathcal{N}\mathcal{C}_1$ score, which increases linearly when adding more classes to each label (i.e., increasing multi-modality). As for the other datasets, *CIFAR-10* is generally more collapsed according to its low value of $\mathcal{N}\mathcal{C}_1$, which even falls below 1 for the Transformer-based FMs. We hypothesize that this is due to the similarity of its categories to those appearing in *ImageNet*. By design, the synthetic *CombiDigits* dataset, introduced in section 4, has a very high $\mathcal{N}\mathcal{C}_1$. Apart from that, $\mathcal{N}\mathcal{C}_1$ of the *ImageNet* data for the Transformer-based architectures are much lower and therefore they are more collapsed compared to the CNN-based FMs. These architectural differences are further investigated in appendix A.4.



(a) A clear linear relationship between the neural collapse measure $\mathcal{N}\mathcal{C}_1$ and d can be inferred for all FMs, i.e., increased multi-modality implies less collapse. The $\mathcal{N}\mathcal{C}_1$ of other datasets (*CombiDigits* in particular) is much higher across all FMs, while only *vit_b_16* and *swin_b* get an $\mathcal{N}\mathcal{C}_1$ of less than one on *CIFAR-10*.

(b) Accuracy over number of proxies k used in *k-means* together with L2 for all *NORM* and *max* as aggregation. In all four subplots, peaks in accuracy at $k = d$ can be inferred. This confirms the connection between the effect of using multiple proxies and the collapse of the data.

Figure 11: Averaged $\mathcal{N}\mathcal{C}_1$ resp. accuracy of ten random *ImageNet* label remappings (“ d in 1”) for every $d = 1, \dots, 10$. Shaded areas indicate 95% CIs over three different seeds. Values for the tasks containing all of *MNIST*, *FashionMNIST*, *CIFAR-10*, resp. *CombiDigits* at once are shown in dotted styles.

For the same data, fig. 11b depicts accuracy over a varying number of proxies k inferred from *k-means*. A prominent peak at $k = d$ can be inferred for every FM and reflects that d class proxies lead to the best result for d -modal class distributions. Furthermore, increasing k for the *ImageNet* sets has a much larger effect on the CNN-based FMs. We argue that this is because of their higher values of $\mathcal{N}\mathcal{C}_1$, indicating less neural collapse. In appendix A.4, we analyze architectural differences and training setups to explain these variations. The fact that *CIFAR-10* has the lowest $\mathcal{N}\mathcal{C}_1$ scores (see fig. 11a) is reflected by flat green curves over k .

Figure 12 renders this connection more precise: For datasets with large \mathcal{NC}_1 , i.e., where intra-class variability surpasses inter-class variability, using more than a single proxy per class ($k > 1$) yields a clear performance gain over mean imprinting ($k = 1$).

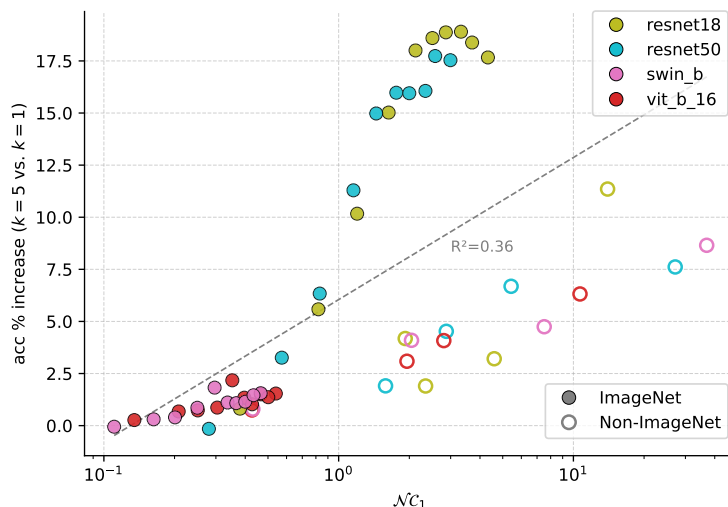


Figure 12: Accuracy (%) gain when using $k = 5$ instead of $k = 1$ proxies per class with **k-means**, plotted against the neural collapse measure \mathcal{NC}_1 (log-scaled axis). Colors indicate different FMs. Outlined markers correspond to non-*ImageNet* datasets (*MNIST*, *FashionMNIST*, *CIFAR-10*, and *CombiDigits*), while filled markers denote averaged results from our random *ImageNet* label remappings. The dashed gray line shows a least-squares fit ($R^2 = 0.36$), summarizing an approximate log-linear dependence between \mathcal{NC}_1 and the gains from using $k > 1$ proxies. Across all points, the Spearman rank correlation is $\rho = 0.82$ ($p < 0.0001$), indicating a statistically significant positive association. Consistent with this trend, for regimes with $\mathcal{NC}_1 > 1$ single-proxy **mean** imprinting ($k = 1$) appears to become substantially suboptimal compared to using multiple proxies ($k > 1$).

6 Conclusion

We present a new framework, **IMPRINT**, to analyze three main components relevant to weight imprinting, namely, weight generation, normalization, and aggregation. Within **IMPRINT**, state-of-the-art imprinting strategies become special cases. This allows for a comprehensive analysis of different approaches through systematic experiments and leads us to generalize to a new, best-performing imprinting variant. That is, using **k-means** weight generation with L2 normalizations and **max** aggregation, which outperforms all previously studied methods (see fig. 2).

k-means generates better weights than mean. In particular, we find that the **mean** weight generation (**GEN**) method, despite its prominence in previous work, falls short compared to **k-means** – even when the number of proxies k is very small. Remarkably, with as little as 50 samples per class, **k-means** can already outperform the original imprinting method proposed by Qi et al. (2018), highlighting its advantage in low-data regimes.

L2 weight normalization is essential for strong performance. The **max** aggregation directly scales with the magnitude of the weights. Normalization (NORM_{post}) ensures that all proxies have the same magnitude, preventing differences in vector norms from disproportionately affecting classifier predictions. Nearest neighbor (**1-nn**) aggregation is not as affected by the lack of normalization, since it uses Euclidean distance. Although still part of common procedure, normalizations for embeddings (NORM_{pre} and NORM_{inf}) appear to have minimal impact on performance.

With max aggregation, there is no need to store all data. While nearest neighbor (m-nn) aggregation (AGG) performs well when all data is saved (e.g., when there are no storage constraints), max aggregation with limited number of representative proxies (e.g., through k -means) is an efficient alternative without a substantial loss in performance.

Neural collapse proves the efficacy of imprinting. During training, the last-layer weights of a FM tend to collapse to their respective class means. This proves the success of **mean** imprinting on known classes. New, out-of-distribution data, however, often shows less collapse, making it beneficial to imprint more than one proxy. Our results show that the advantage of using multiple proxies is strongly coupled to the degree of neural collapse: the accuracy gain from using $k > 1$ proxies increases approximately log-linearly with \mathcal{NC}_1 . In particular, multi-proxy imprinting yields substantial and predictable improvements on datasets with \mathcal{NC}_1 exceeding 1. While from a practical perspective, choosing the exact number of proxies k based on pure greedy search with validation data (or as part of any AutoML pipeline) is still a valid option, our analysis provides insights into the underlying mechanism, turning \mathcal{NC}_1 into an indicator for when multi-proxy imprinting is highly beneficial.

Limitations. Our experiments are limited to foundation models for image classification and do not cover other data modalities such as audio, text, or sensor inputs. While IMPRINT is agnostic to modality, empirical validation of our results outside of vision is needed. Although imprinting alone provides an efficient solution to transfer learning, when compared to purely gradient-based learning, a gap still remains. We do not investigate the benefit of combining it with optimization methods such as gradient-based learning, and the choice of k still requires heuristic or empirical selection rather than direct prediction.

Future Work. The usage of both weight and activation sparsity as Shen et al. (2023) could change the within- and between-class variability in favor of using a higher number of proxies. Besides only using the penultimate layer embeddings for generating the classifier weights, an interesting area of study could be extracting embeddings from previous layers of the FM for this purpose. Recently, the study by Marczak et al. (2025) showed that adding a multi-layer perceptron projector between the penultimate and classification layers results in representations that are more transferable. Another avenue of research is to thoroughly analyze imprinting the weights of other layers as well (Siam et al., 2019).

Acknowledgments

Our work is funded by the Deutsche Forschungsgemeinschaft (DFG, German Research Foundation) – FIP-12 – Project-ID 528483508, as well as the European Union under the grant project 101079894 (COMFORT - Improving Urologic Cancer Care with Artificial Intelligence Solutions). Views and opinions expressed are however those of the author(s) only and do not necessarily reflect those of the European Union or European Health and Digital Executive Agency (HADEA). Neither the European Union nor the granting authority can be held responsible for them. We thank Viet Anh Khoa Tran for initial discussions about the neural collapse phenomenon. We further thank the reviewers and the Action Editor for their detailed and constructive feedback, which substantially improved this work.

Author Contributions

JW contributed to the development of the framework, conducting experiments and evaluated the findings. GA was responsible for investigating NC measures and overall contribution to the project. MK contributed to extending the framework and handling data preparation. AF provided critical feedback on the presentation of the results and contributed to refining the manuscript. AL, ER, and FG provided supervision, contributed to the overall concepts presented, and to refining the manuscript.

References

- Dhammika Amaratunga and Javier Cabrera. Analysis of data from viral dna microchips. *Journal of the American Statistical Association*, 96(456):1161–1170, 2001.
- James A Anderson. A simple neural network generating an interactive memory. *Mathematical biosciences*, 14(3-4): 197–220, 1972.
- James A Anderson, Jack W Silverstein, Stephen A Ritz, and Randall S Jones. Distinctive features, categorical perception, and probability learning: Some applications of a neural model. *Psychological review*, 84(5):413, 1977.
- Maximilian Beck, Korbinian Pöppel, Markus Spanring, Andreas Auer, Oleksandra Prudnikova, Michael Kopp, Günter Klambauer, Johannes Brandstetter, and Sepp Hochreiter. xlstm: Extended long short-term memory. In Amir Globersons, Lester Mackey, Danielle Belgrave, Angela Fan, Ulrich Paquet, Jakub M. Tomczak, and Cheng Zhang (eds.), *Advances in Neural Information Processing Systems 38: Annual Conference on Neural Information Processing Systems 2024, NeurIPS 2024, Vancouver, BC, Canada, December 10 - 15, 2024*, 2024. URL http://papers.nips.cc/paper_files/paper/2024/hash/c2ce2f2701c10a2b2f2ea0bfa43cfaa3-Abstract-Conference.html.
- Mohammad Belal, Taimur Hassan, Abdelfatah Hassan, Divya Velayudhan, Noureldin Elhendawi, Ahmad Aljarah, and Irfan Hussain. Fsid: a novel approach to human activity recognition using few-shot weight imprinting. *Scientific Reports*, 15(1):20865, 2025.
- Yoshua Bengio. Deep learning of representations for unsupervised and transfer learning. In *Proceedings of ICML workshop on unsupervised and transfer learning*, pp. 17–36. JMLR Workshop and Conference Proceedings, 2012.
- Benjamin M Bolstad, Rafael A Irizarry, Magnus Åstrand, and Terence P. Speed. A comparison of normalization methods for high density oligonucleotide array data based on variance and bias. *Bioinformatics*, 19(2):185–193, 2003.
- Rishi Bommasani, Drew A Hudson, Ehsan Adeli, Russ Altman, Simran Arora, Sydney von Arx, Michael S Bernstein, Jeannette Bohg, Antoine Bosselut, Emma Brunskill, et al. On the opportunities and risks of foundation models. *arXiv preprint arXiv:2108.07258*, 2021.
- Google Coral. Retrain a classification model on-device with weight imprinting. <https://coral.ai/docs/edgetpu/retrain-classification-ondevice>.
- Paulino Cristovao, Hidemoto Nakada, Yusuke Tanimura, and Hideki Asoh. Few shot model based on weight imprinting with multiple projection head. In *2022 16th International Conference on Ubiquitous Information Management and Communication (IMCOM)*, pp. 1–7. IEEE, 2022.
- Peter Dayan and David J Willshaw. Optimising synaptic learning rules in linear associative memories. *Biological cybernetics*, 65(4):253–265, 1991.
- Janez Demšar. Statistical comparisons of classifiers over multiple data sets. *The Journal of Machine learning research*, 7:1–30, 2006.
- Jia Deng, Wei Dong, Richard Socher, Li-Jia Li, Kai Li, and Li Fei-Fei. Imagenet: A large-scale hierarchical image database. In *2009 IEEE conference on computer vision and pattern recognition*, pp. 248–255, 2009.
- Li Deng. The mnist database of handwritten digit images for machine learning research [best of the web]. *IEEE signal processing magazine*, 29(6):141–142, 2012.
- Jacob Devlin, Ming-Wei Chang, Kenton Lee, and Kristina Toutanova. BERT: Pre-training of Deep Bidirectional Transformers for Language Understanding. In *NAACL-HLT*, pp. 4171–4186, 2019.
- Jeff Donahue, Yangqing Jia, Oriol Vinyals, Judy Hoffman, Ning Zhang, Eric Tzeng, and Trevor Darrell. DeCAF: A Deep Convolutional Activation Feature for Generic Visual Recognition. In *ICML*, pp. 647–655, 2014.
- Alexey Dosovitskiy, Lucas Beyer, Alexander Kolesnikov, Dirk Weissenborn, Xiaohua Zhai, Thomas Unterthiner, Mostafa Dehghani, Matthias Minderer, Georg Heigold, Sylvain Gelly, et al. An image is worth 16x16 words: Transformers for image recognition at scale. In *International Conference on Learning Representations*, 2021.
- Tomer Galanti, András György, and Marcus Hutter. On the role of neural collapse in transfer learning. In *International Conference on Learning Representations*, 2022.

- Yaroslav Ganin, Evgeniya Ustinova, Hana Ajakan, Pascal Germain, Hugo Larochelle, François Laviolette, Mario March, and Victor Lempitsky. Domain-adversarial training of neural networks. *Journal of machine learning research*, 17(59):1–35, 2016.
- Spyros Gidaris and Nikos Komodakis. Dynamic few-shot visual learning without forgetting. In *Proceedings of the IEEE conference on computer vision and pattern recognition*, pp. 4367–4375, 2018.
- X. Y. Han, Vardan Papyan, and David L. Donoho. Neural collapse under MSE loss: Proximity to and dynamics on the central path. In *The Tenth International Conference on Learning Representations, ICLR, 2022*.
- Md Yousuf Harun and Christopher Kanan. A good start matters: Enhancing continual learning with data-driven weight initialization. *arXiv preprint arXiv:2503.06385*, 2025.
- Kaiming He, Xiangyu Zhang, Shaoqing Ren, and Jian Sun. Deep residual learning for image recognition. In *Proceedings of the IEEE conference on computer vision and pattern recognition*, pp. 770–778, 2016.
- Sture Holm. A simple sequentially rejective multiple test procedure. *Scandinavian journal of statistics*, pp. 65–70, 1979.
- Kazufumi Hosoda, Keigo Nishida, Shigeto Seno, Tomohiro Mashita, Hideki Kashioka, and Izumi Ohzawa. A single fast hebbian-like process enabling one-shot class addition in deep neural networks without backbone modification. *Frontiers in Neuroscience*, 18:1344114, 2024.
- Minyoung Huh, Pulkit Agrawal, and Alexei A. Efros. What makes ImageNet good for transfer learning?, 2016. arXiv:1608.08614.
- Jonathan J. Hull. A database for handwritten text recognition research. *IEEE Transactions on pattern analysis and machine intelligence*, 16(5):550–554, 1994.
- Hassan Ismail Fawaz, Germain Forestier, Jonathan Weber, Lhassane Idoumghar, and Pierre-Alain Muller. Deep learning for time series classification: a review. *Data mining and knowledge discovery*, 33(4):917–963, 2019.
- Paul Janson, Wenxuan Zhang, Rahaf Aljundi, and Mohamed Elhoseiny. A simple baseline that questions the use of pretrained-models in continual learning. In *NeurIPS 2022 Workshop on Distribution Shifts: Connecting Methods and Applications*, 2022.
- Mina Khan, P Srivatsa, Advait Rane, Shriram Chenniappa, Asadali Hazariwala, and Pattie Maes. Personalizing pre-trained models. *arXiv preprint arXiv:2106.01499*, 2021.
- Teuvo Kohonen. Correlation matrix memories. *IEEE transactions on computers*, 100(4):353–359, 2009.
- Simon Kornblith, Jonathon Shlens, and Quoc V. Le. Do Better ImageNet Models Transfer Better? In *CVPR*, pp. 2656–2666, Long Beach, CA, USA, 2019. IEEE.
- Vignesh Kothapalli. Neural collapse: A review on modelling principles and generalization. *Transactions on Machine Learning Research*, 2023. ISSN 2835-8856.
- Alex Krizhevsky, Geoffrey Hinton, et al. CIFAR-10. <https://www.cs.toronto.edu/~kriz/cifar.html>, 2009.
- Yiting Li, Haiyue Zhu, Jun Ma, Sichao Tian, Chek Sing Teo, Cheng Xiang, Prahlad Vadakkepa, and Tong Heng Lee. Classification weight imprinting for data efficient object detection. In *2021 IEEE 30th International Symposium on Industrial Electronics (ISIE)*, pp. 1–5. IEEE, 2021.
- Ze Liu, Yutong Lin, Yue Cao, Han Hu, Yixuan Wei, Zheng Zhang, Stephen Lin, and Baining Guo. Swin transformer: Hierarchical vision transformer using shifted windows. In *Proceedings of the IEEE/CVF international conference on computer vision*, pp. 10012–10022, 2021.
- Daniel Marczak, Sebastian Cygert, Tomasz Trzcíński, and Bartłomiej Twardowski. Revisiting supervision for continual representation learning. In *European Conference on Computer Vision*, pp. 181–197. Springer, 2025.
- Thomas Mensink, Jakob Verbeek, Florent Perronnin, and Gabriela Csurka. Distance-based image classification: Generalizing to new classes at near-zero cost. *IEEE transactions on pattern analysis and machine intelligence*, 35(11):2624–2637, 2013.

- Yair Movshovitz-Attias, Alexander Toshev, Thomas K Leung, Sergey Ioffe, and Saurabh Singh. No fuss distance metric learning using proxies. In *Proceedings of the IEEE international conference on computer vision*, pp. 360–368, 2017.
- Kaoru Nakano. Associatron—a model of associative memory. *IEEE Transactions on systems, man, and cybernetics*, pp. 380–388, 2007.
- Yuval Netzer, Tao Wang, Adam Coates, Alessandro Bissacco, Baolin Wu, Andrew Y Ng, et al. Reading digits in natural images with unsupervised feature learning. In *NIPS workshop on deep learning and unsupervised feature learning*, volume 2011, pp. 4. Granada, 2011.
- Vardan Pappayan, XY Han, and David L Donoho. Prevalence of neural collapse during the terminal phase of deep learning training. *Proceedings of the National Academy of Sciences*, 117(40):24652–24663, 2020.
- Nikolaos Passalis, Alexandros Iosifidis, Moncef Gabbouj, and Anastasios Tefas. Hypersphere-based weight imprinting for few-shot learning on embedded devices. *IEEE Transactions on Neural Networks and Learning Systems*, 32(2): 925–930, 2020.
- F. Pedregosa, G. Varoquaux, A. Gramfort, V. Michel, B. Thirion, O. Grisel, M. Blondel, P. Prettenhofer, R. Weiss, V. Dubourg, J. Vanderplas, A. Passos, D. Cournapeau, M. Brucher, M. Perrot, and E. Duchesnay. Scikit-learn: Machine learning in Python. *Journal of Machine Learning Research*, 12:2825–2830, 2011.
- Ameya Prabhu, Zhipeng Cai, Puneet Dokania, Philip Torr, Vladlen Koltun, and Ozan Sener. Online continual learning without the storage constraint. *arXiv preprint arXiv:2305.09253*, 2023.
- Hang Qi, Matthew Brown, and David G Lowe. Low-shot learning with imprinted weights. In *Proceedings of the IEEE conference on computer vision and pattern recognition*, pp. 5822–5830, 2018.
- Sylvestre-Alvise Rebuffi, Alexander Kolesnikov, Georg Sperl, and Christoph H Lampert. icarl: Incremental classifier and representation learning. In *Proceedings of the IEEE conference on Computer Vision and Pattern Recognition*, pp. 2001–2010, 2017.
- Terrence J Sejnowski. Storing covariance with nonlinearly interacting neurons. *Journal of mathematical biology*, 4(4): 303–321, 1977.
- Yang Shen, Sanjoy Dasgupta, and Saket Navlakha. Reducing catastrophic forgetting with associative learning: a lesson from fruit flies. *Neural Computation*, 35(11):1797–1819, 2023.
- Mennatullah Siam, Boris N Oreshkin, and Martin Jagersand. Amp: Adaptive masked proxies for few-shot segmentation. In *Proceedings of the IEEE/CVF International Conference on Computer Vision*, pp. 5249–5258, 2019.
- Jake Snell, Kevin Swersky, and Richard Zemel. Prototypical networks for few-shot learning. *Advances in neural information processing systems*, 30, 2017.
- Tom Tirer, Haoxiang Huang, and Jonathan Niles-Weed. Perturbation analysis of neural collapse. In *International Conference on Machine Learning*, pp. 34301–34329. PMLR, 2023.
- Han Xiao, Kashif Rasul, and Roland Vollgraf. Fashion-mnist: a novel image dataset for benchmarking machine learning algorithms. *arXiv preprint arXiv:1708.07747*, 2017.
- Dingtian Yan, Jitao Huang, Hai Sun, and Fuqiang Ding. Few-shot object detection with weight imprinting. *Cognitive Computation*, 15(5):1725–1735, 2023.
- Hong-Ming Yang, Xu-Yao Zhang, Fei Yin, and Cheng-Lin Liu. Robust classification with convolutional prototype learning. In *Proceedings of the IEEE conference on computer vision and pattern recognition*, pp. 3474–3482, 2018.
- Jason Yosinski, Jeff Clune, Yoshua Bengio, and Hod Lipson. How transferable are features in deep neural networks? *Advances in neural information processing systems*, 27, 2014.
- Lu Yu, Bartłomiej Twardowski, Xialei Liu, Luis Herranz, Kai Wang, Yongmei Cheng, Shangling Jui, and Joost van de Weijer. Semantic drift compensation for class-incremental learning. In *Proceedings of the IEEE/CVF conference on computer vision and pattern recognition*, pp. 6982–6991, 2020.
- Jianxing Zhang, Pengcheng Xi, Ashkan Ebadi, Hilda Azimi, Stéphane Tremblay, and Alexander Wong. Covid-19 detection from chest x-ray images using imprinted weights approach. *arXiv preprint arXiv:2105.01710*, 2021.

Haiyue Zhu, Xiong Li, Wenjie Chen, Xiacong Li, Jun Ma, Chek Sing Teo, Tat Joo Teo, and Wei Lin. Weight imprinting classification-based force grasping with a variable-stiffness robotic gripper. *IEEE Transactions on Automation Science and Engineering*, 19(2):969–981, 2022.

Zhihui Zhu, Tianyu Ding, Jinxin Zhou, Xiao Li, Chong You, Jeremias Sulam, and Qing Qu. A geometric analysis of neural collapse with unconstrained features. *Advances in Neural Information Processing Systems*, 34:29820–29834, 2021.

A Appendix

A.1 Additional Results

We provide additional tables and critical difference (CD) diagrams that expand on the results of section 5.

Table A.1 & Figure A.1: Benchmarking GEN mechanism for $k \leq 5$ across FMs and Ts. Best NORM combination for each row is used implicitly. AGG is fixed to max. CD diagram depicts statistical significance of **k-means** as GEN. See fig. 5 for $k \leq 20$.

GEN	k	Avg. acc. % \pm std
k-means	5	89.15 \pm 6.96
mean	1	86.84 \pm 7.80
k-medoids	5	84.87 \pm 8.76
k-cov-max	5	82.11 \pm 10.39
k-random	5	75.93 \pm 11.92
k-fps	5	63.64 \pm 12.29

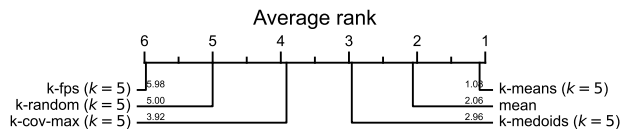


Table A.2 & Figure A.2: Benchmarking NORM across FMs and Ts shows crucial effect of L2 normalization. GEN is fixed to mean and AGG to max. CD diagram depicting statistical significance of L2 for $NORM_{post}$. Combinations are listed as “ $NORM_{inf}$ & $NORM_{pre}$ & $NORM_{post}$ ”.

$NORM_{inf}$	$NORM_{pre}$	$NORM_{post}$	Avg. acc. % \pm std
L2	none	L2	86.84 \pm 7.80
none	none	L2	86.84 \pm 7.80
L2	L2	L2	86.79 \pm 7.83
L2	none	quantile	82.90 \pm 12.87
none	none	quantile	82.90 \pm 12.87
L2	L2	quantile	82.83 \pm 12.86
L2	L2	none	83.26 \pm 9.18
L2	none	none	67.66 \pm 22.12
none	none	none	67.66 \pm 22.12

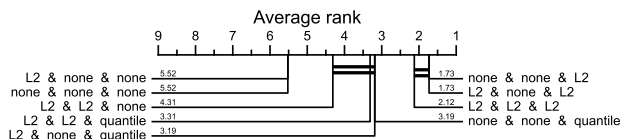
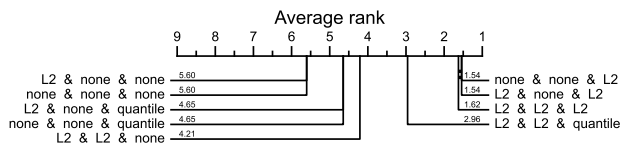


Table A.3 & Figure A.3: Benchmarking NORM across FMs and Ts. GEN is fixed to k-means with $k = 20$ and AGG to max. CD diagram depicting statistical significance of L2 for $NORM_{post}$. Combinations are listed as “ $NORM_{inf}$ & $NORM_{pre}$ & $NORM_{post}$ ”.

$NORM_{inf}$	$NORM_{pre}$	$NORM_{post}$	Avg. acc. % \pm std
L2	none	L2	91.04 \pm 6.26
none	none	L2	91.04 \pm 6.26
L2	L2	L2	91.06 \pm 6.21
L2	L2	quantile	90.51 \pm 6.40
L2	L2	none	89.55 \pm 6.70
L2	none	quantile	79.21 \pm 15.20
none	none	quantile	79.21 \pm 15.20
L2	none	none	73.53 \pm 21.05
none	none	none	73.53 \pm 21.05



A.2 Datasets

We briefly describe the datasets used in our experiments.

ImageNet (Deng et al., 2009). We use the ILSVRC 2012 version (commonly called *ImageNet-1K*) containing 1000 classes and 1.2M training images. Since the test set is not publicly available, we use the

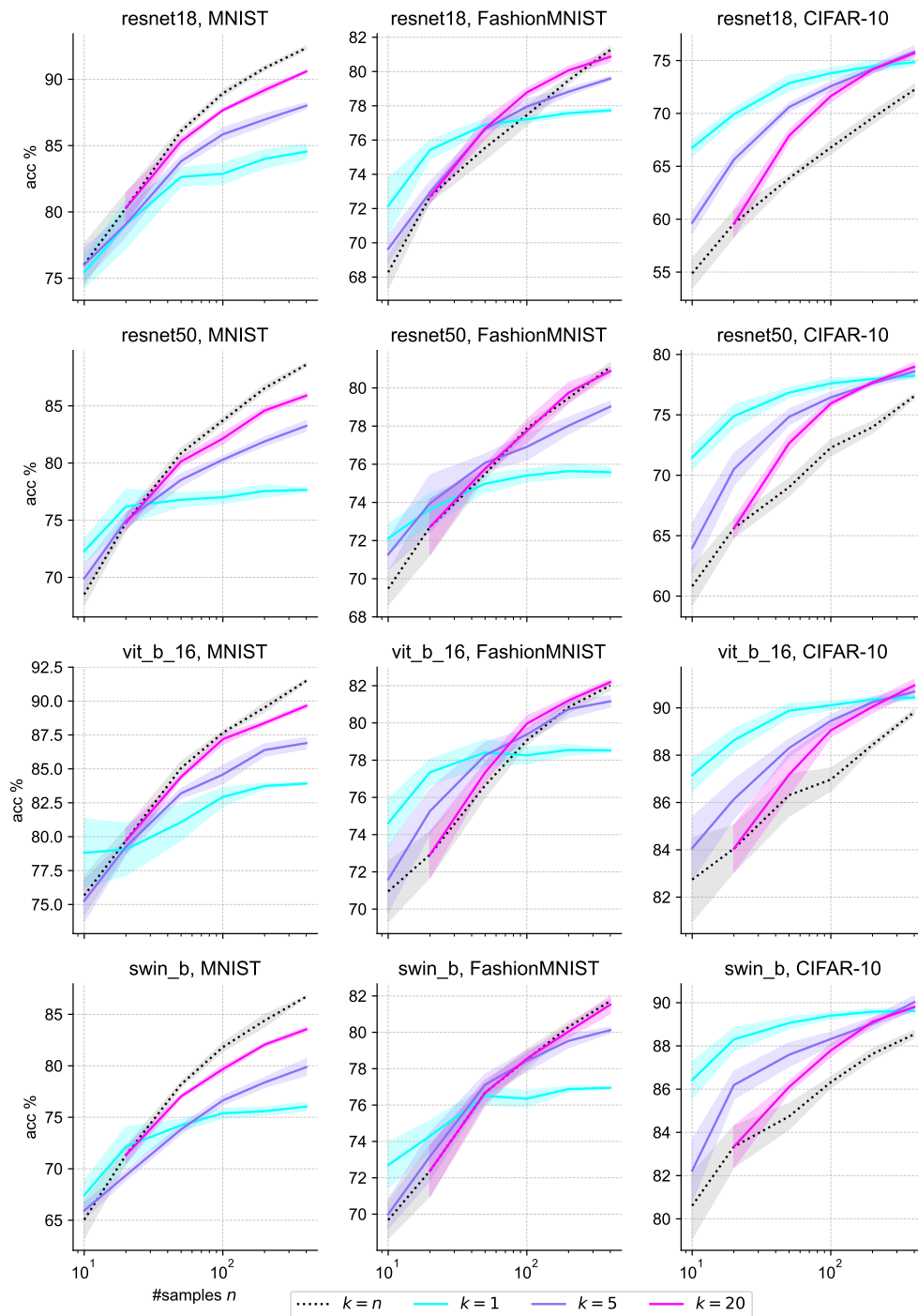


Figure A.4: k-means with different values for k in n -shot scenarios with focus on $10 \leq n \leq 400$. Shaded areas indicate 95% confidence intervals (CIs) over five different seeds. Other variables are fixed to our previously described best method of using L2 for NORM and max as AGG. Note that only data for the meaningful case of $k \leq n$ is shown. For *MNIST* and *FashionMNIST*, mean ceases to be the best strategy already at only roughly 50 samples. See fig. 10 for more values of n .

validation set (50 000 images) as a stand-in. For neural collapse investigations, we construct tasks by randomly grouping d classes into one label, producing “ d in 1” tasks as explained in section 4.

***MNIST* (Deng, 2012).** A benchmark dataset of handwritten digits (0–9), consisting of 60 000 training and 10 000 test grayscale images of size 28×28 .

***FashionMNIST* (Xiao et al., 2017).** A drop-in replacement for *MNIST* with the same format and number of samples, containing grayscale images of fashion items across 10 classes.

***CIFAR-10* (Krizhevsky et al., 2009).** A dataset of 32×32 RGB images covering 10 object classes, with 50 000 training and 10 000 test samples.

***MNIST-M* (Ganin et al., 2016), *SVHN* (Netzer et al., 2011), *USPS* (Hull, 1994).** Digit classification datasets each containing digits 0-9 with domain-specific visual characteristics. *MNIST-M* applies color and texture transformations to *MNIST* digits, yielding 60 000 training and 10 000 RGB images of size 28×28 . *SVHN* consists of digit crops from house numbers in Google Street View, totaling 73 257 training and 26 032 test images of 32×32 in RGB. *USPS* contains scanned and normalized handwritten digits in 16×16 grayscale, split into 7 219 training and 2 007 test images.

***CombiDigits* (Ours).** A synthetic dataset constructed by merging all classes from *MNIST*, *MNIST-M*, *SVHN*, and *USPS*. Each class label corresponds to a digit (0–9) and fig. A.5 shows example images of class “6”. The dataset includes significant visual heterogeneity across sources and thus simulates multi-modal, non-collapsed class distributions.



Figure A.5: Twenty sample images from class “6” of the *CombiDigits* dataset. Each row corresponds to one of the four source datasets: *MNIST*, *MNIST-M*, *SVHN*, and *USPS* (top to bottom), illustrating the intra-class heterogeneity across domains.

A.3 Imprinting as Memory

We revisit the classical idea of Bidirectional Associative Memories (BAMs) (Kohonen, 2009; Anderson, 1972; Nakano, 2007; Anderson et al., 1977) and the associated update rule (Sejnowski, 1977; Dayan & Willshaw, 1991) for storing key-value pairs as in

$$\mathbf{W} \leftarrow \mathbf{W} + \mathbf{v}\mathbf{k}^\top,$$

where $\mathbf{W} \in \mathbb{R}^{l \times l}$ is a matrix and $\mathbf{k}, \mathbf{v} \in \mathbb{R}^d$ are key and value vectors, respectively, to be stored therein.

Throughout this work, imprinting can be interpreted as inserting such key-value associations into the classifier weights. More precisely, the generation (GEN) component extends the linear classification head by setting \mathbf{v}

as a one-hot vector representing the class, and \mathbf{k} as the corresponding proxy previously computed. While we focus on this simple linear setting, imprinting is not limited to it, as discussed in section 2.

Notably, this form of direct memory update has seen renewed attention in modern architectures beyond standard query-key-value attention. In particular, the xLSTM model (Beck et al., 2024) implements this mechanism within its mLSTM memory blocks, where the matrix memory cell is updated by gated key-value associations, closely following this classical covariance rule, indicating a broader resurgence of associative memory principles in contemporary sequence modeling.

A.4 Differences between Foundation Models

While an in-depth comparison of foundation models is beyond the scope of this work, we believe it is important to highlight key observations we have made. In particular, fig. 11a shows significantly lower \mathcal{NC}_1 scores for `vit_b_16` and `swin_b` on their pre-training *ImageNet* data compared to the `resnet` models. We hypothesize that this difference is primarily due to model size and training regimes. The Transformer-based architectures (`vit_b_16` and `swin_b`) have a considerably higher parameter count ($\approx 87\text{M}$) than the `resnet` models (11.7M and 25.6M, respectively). Additionally, `vit_b_16` and `swin_b` were trained for more than three times as many epochs (300 vs. 90) while using a substantially lower learning rate (0.003 and 0.01 vs. 0.1). Notably, the embedding dimensions of these models are comparable, meaning that the observed differences in \mathcal{NC}_1 scores cannot be attributed to differences in representation dimensionality. Instead, we argue that the combination of larger model size, extended training duration, and lower learning rates likely contributes to greater overfitting, leading to more pronounced collapse. As discussed in section 5.3, this enables the Transformer-based FMs to handle the *ImageNet* tasks with remapped labels more effectively and to achieve significantly better performance on the similarly distributed *CIFAR-10* dataset.

Figure A.6a, similar to fig. 11b, illustrates the impact of varying the number of proxies on imprinting accuracy across different foundation models (FMs). The key difference in this figure is the use of `none` for NORM_{pre} instead of `L2`. This seemingly minor change reveals a striking contrast between CNN- and Transformer-based architectures: a distinct and consistent dip between $k = 1$ and $k = d$ appears in Transformer-based models, whereas this dip is absent in fig. 11b, where `L2` is used as NORM_{pre} , and does not occur at all in the `resnet` models. We hypothesize that this difference arises from the distinct embedding distributions of CNN- and Transformer-based architectures (see, e.g., Hosoda et al. (2024, Figure S2)).

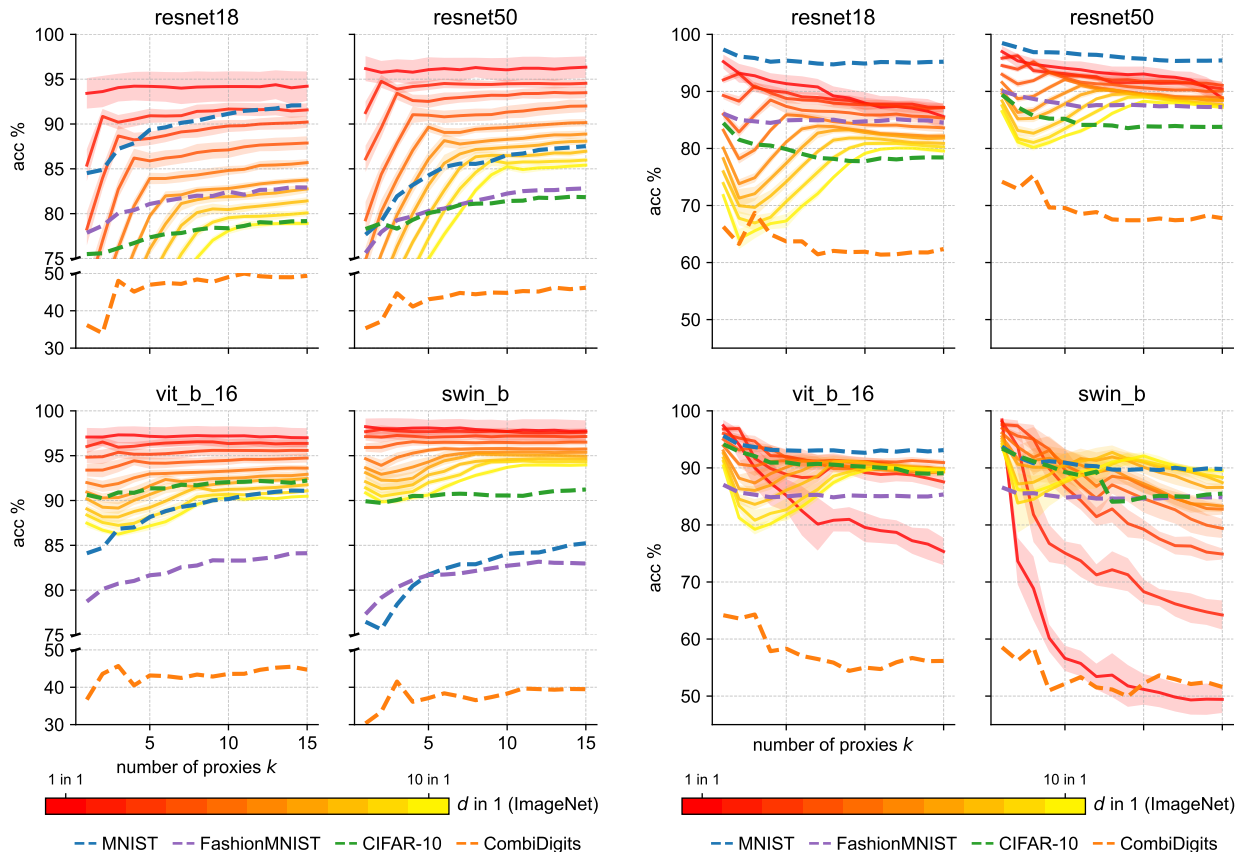
A.5 Learned Weights (with Multiple Proxies) and Comparisons

Harun & Kanan (2025) recently studied the initialization of classifier weights for novel categories in a Continual Learning (CL) setting using the least squares algorithm, comparing it to random initialization and class mean imprinting across various loss functions. In contrast, our work centers on imprinting-based approaches, which avoid using gradient-based optimization and cross-class statistics, operating instead on a per-class basis with immediate availability of data. Nonetheless, we include the least-squares method as a supervised oracle baseline – explicitly not an imprinting method – fine-tuned for classification accuracy.

We evaluate the performance of `least-squares` on the same tasks as defined in section 4. Additionally, we introduce a multi-proxy extension, `k-least-squares`, which combines least squares with `k-means` clustering. As in the case of weight generation `GEN` in imprinting (where `k-means` outperforms `mean`), we find that using multiple proxies per class improves performance in settings with high \mathcal{NC}_1 as well, indicating that the benefits of multi-prototype representations persist even in this non-imprinting, supervised context.

All experiments use no normalization (`none` as NORM), based on ablations confirming that additional normalization impairs performance. This matches expectations, since least squares outputs are already calibrated, and normalization distorts them.

Least Squares Weights. For all data contained in task \mathbf{T} , define $\mathbf{H} \in \mathbb{R}^{l \times N}$ as the collection of all feature vectors of the N training samples in \mathbf{T} obtained by applying a fixed FM, i.e., $\mathbf{h}_{c,i} \in \mathbb{R}^l$ is the feature vector of the i -th sample in the c -th class. Recall from section 3.2 that the within-class covariance matrix Σ_W is given as $\mathbb{E}_{c,i}[(\mathbf{h}_{c,i} - \bar{\mathbf{h}}_c)(\mathbf{h}_{c,i} - \bar{\mathbf{h}}_c)^\top]$ and additionally define the total covariance matrix Σ_T and the class-means



(a) **k-means** used as GEN. $NORM_{post}$ and $NORM_{inf}$ are set to L2, and $NORM_{pre}$ to none. Besides the prominent peaks in accuracy at $k = d$ (as already observed in fig. 11b), a consistent dip between $k = 1$ and $k = d$ appears in Transformer-based models, which was not to be seen with $NORM_{pre}$ set to L2 as well. In appendix A.4 we hypothesize that this is due to the distinct embeddings distributions of CNN- and Transformer-based architectures.

(b) **k-least-squares** (see appendix A.5) used as GEN and all $NORM$ are set to none. Here, the CNN-based FMs exhibit a clear accuracy peak at $k = d$, with a consistent drop for intermediate values $1 < k < d$. For the Transformer-based FMs, however, accuracy is typically highest at $k = 1$ and only improves slightly around $k = d$ but does not show a pronounced peak. For all FMs, performance declines with $k > d$, indicating that excessive proxy splitting harms generalization. This degradation does not occur in **k-means** GEN, which remains robust even with large k (see figs. 11b and A.6a).

Figure A.6: Averaged accuracy of ten random *ImageNet* label remappings (“ d in 1”) for every $d = 1, \dots, 10$ over number of proxies k . Shaded areas indicate 95% CIs over three different seeds. Values for the tasks containing all of *MNIST*, *FashionMNIST*, *CIFAR-10*, resp. *CombiDigits* at once are shown in dotted lines.

matrix \mathbf{M} as

$$\mathbf{M} = [\bar{\mathbf{h}}_1, \dots, \bar{\mathbf{h}}_C] \in \mathbb{R}^{l \times C}, \quad \Sigma_T = \mathbb{E}_{c,i}[(\mathbf{h}_{c,i} - \mathbf{h}_G)(\mathbf{h}_{c,i} - \mathbf{h}_G)^\top] \in \mathbb{R}^{l \times l}.$$

From these feature statistics, we can obtain the **least-squares** weights via

$$\mathbf{W}_{LS} = \frac{1}{C} \mathbf{M}^\top (\Sigma_T + \mathbf{h}_G \mathbf{h}_G^\top + \lambda \mathbf{I})^{-1}. \tag{A.1}$$

Here, \mathbf{I} is the identity matrix and λ is the weight decay. We set λ to match the value used during the original training of each respective model. Table A.4 lists the specific λ values used for all models considered in our experiments.

Table A.4: Weight decay values λ used for each model.

Model	λ
resnet18, resnet50 (He et al., 2016)	0.0001
vit_b_16 (Dosovitskiy et al., 2021)	0.1
swin_b (Liu et al., 2021)	0.05

Equation (A.1) reveals that **least-squares** shares structural similarities with **mean** imprinting, but applies a more sophisticated normalization scheme that includes both scaling and rotation. Crucially, it relies on cross-class statistics computed across the entire dataset, and thus is incompatible with imprinting scenarios, which operate by directly constructing class weights from the data of a single class without supervision or access to other classes.

Algorithm 1 k-least-squares

Input: Class data $\{\mathbf{H}_c\}_{c=1}^C$, number of proxies k

Output: Weights $\{\mathbf{W}_c\}_{c=1}^C$ with shape $[k, l]$ per class

- 1: **if** $k = 1$ **then**
 - 2: **return** standard least squares weights \mathbf{W}_{LS} for each class (see eq. (A.1))
 - 3: **end if**
 - 4: **for** each class c **do**
 - 5: Cluster \mathbf{H}_c into k clusters via k -means
 - 6: Assign each cluster j to proxy class (c, j)
 - 7: Collect proxy samples $\{\mathbf{H}_{(c,j)}\}_{j=1}^k$
 - 8: **end for**
 - 9: Compute least squares weights $\mathbf{w}_{(c,j)}$ jointly for all proxy classes (c, j)
 - 10: Assemble $\mathbf{W}_c = [\mathbf{w}_{(c,1)}, \dots, \mathbf{w}_{(c,k)}]$ for each original class c
 - 11: **return** $\{\mathbf{W}_c\}_{c=1}^C$
-

Combining k-means and least-squares into k-least-squares. To allow for multiple proxies per class, we propose **k-least-squares**, a generalization of standard least squares (**least-squares**) that integrates clustering. Instead of computing a single weight vector per class using all class samples, we first partition each class’s feature set \mathbf{H}_c into k clusters using k -means. Each cluster is treated as a separate proxy class, effectively expanding the classification task from C to $k \cdot C$ proxy classes. We then solve a single regularized least squares problem over all proxy classes at once, assigning a distinct target vector to each proxy. The resulting weights are grouped by their original class to yield k weight vectors per class. The complete procedure is given in algorithm 1.

The results in fig. A.6b extend previous findings from **mean** and **k-means** for the CNN-based FMs, as accuracy increases with increasing proxy count k , peaks at $k = d$, and reveals a distinct dip between $k = 1$ and $k = d$, confirming the weakness of using only one proxy per class. For Transformer-based FMs, by contrast, accuracy is often highest at $k = 1$, improves slightly near $k = d$, but lacks a pronounced peak. Beyond $k > d$, accuracy generally declines for **k-least-squares**, indicating diminishing returns from excessive proxy splitting. In contrast, **k-means GEN** maintains stable performance even as k grows, demonstrating robustness to increasing proxy counts.

Comparison with k-means. We now compare the performance of **k-means** and **k-least-squares** as proxy generation methods, noting again that **k-least-squares** is not an imprinting scheme as it does not operate on a class-by-class basis as the imprinting methods presented in section 3.1 do.

Upon proper comparison of the best performing **k-means** and **k-least-squares** configurations, as depicted in fig. A.7, we observe that on our synthetic *ImageNet* tasks, **k-least-squares** does not consistently offer a substantial improvement. In fact, it is only on **resnet50**, in a highly multi-modal setting ($d = 10$), that

k-least-squares reaches better accuracy. For the Transformer-based models, **k-means** even performs better in these scenarios.

While the Transformer-based models generally achieve superior performance overall (note the different y-axis scales for CNN- and Transformer-based models in fig. A.7), a consistent trend across all models is observed: with increasing multi-modality (increasing d), using more than one proxy, whether through **k-means** or **k-least-squares**, begins to outperform the single-proxy methods (**mean** and **least-squares**). Still, it is striking to see how effective single weights with **least-squares** can be. However, it is also noteworthy how easily **k-means** can bridge this gap, particularly considering that **least-squares** is not an actual imprinting scheme, while **k-means** is.

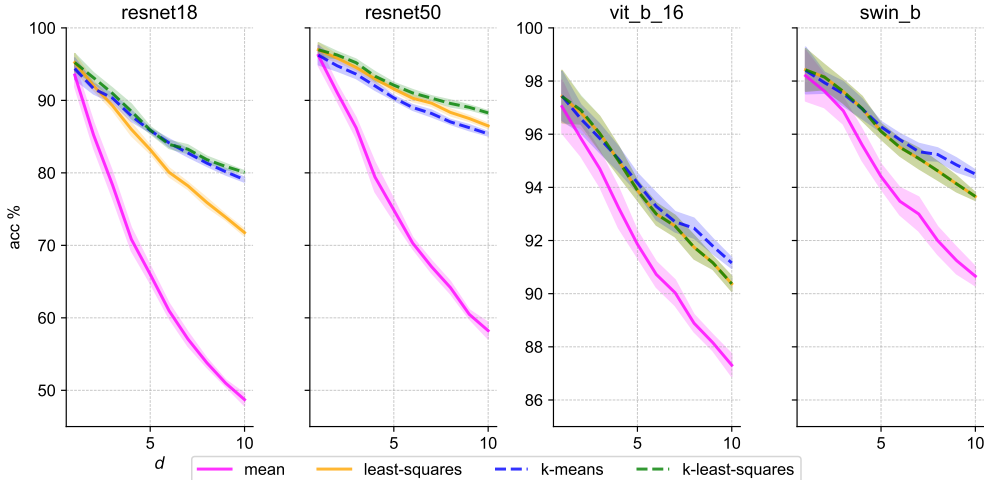


Figure A.7: Averaged accuracy of ten random *ImageNet* label remappings (“ d in 1”) for every $d = 1, \dots, 10$ for **mean** and **least-squares**, and optimal **k-means** and **k-least-squares** ($k \in \{0, \dots, 15\}$) weights. Shaded areas indicate 95% CIs over three different seeds. Note the differing y-axis scales for CNN-based (**resnet18**, **resnet50**) and Transformer-based (**vit_b_16**, **swin_b**) models. The figure illustrates that with increasing multi-modality d , multi-proxy methods (**k-means**, **k-least-squares**) generally outperform single-proxy methods (**mean**, **least-squares**), and that the **k-means** imprinting scheme is competitive with **least-squares** approaches.

Furthermore, we evaluate the **k-least-squares** weight generation method (using **none** for all NORM) across the 48 tasks proposed in the main part of our paper (see section 4). **least-squares** reaches an average accuracy of 94.54%, while **20-least-squares drops** to 91.20%. The observed decrease in accuracy can be explained by the dynamics shown in fig. A.6b. In comparison to the numbers presented in fig. 2, this shows that our **k-means** imprinting scheme significantly bridges the gap between single-proxy imprinting ($k = 1$) and the optimal least squares weights.

A.6 Computational Efficiency

Clustering-based imprinting. Our **k-means** implementation in GEN uses `sklearn.cluster.KMeans` with its default parameters. The cost is $\mathcal{O}(Nklt)$ for N samples, k clusters, feature dimension l , and t Lloyd iterations. While **k-means** is not computationally negligible, both assignment and update steps in each iteration parallelize naturally, and convergence typically requires only a few iterations. Similarly, the other steps in our imprinting framework (**NORM**, **AGG**) scale linearly with dataset size or proxy count and parallelize efficiently, resulting in no practical scalability bottlenecks even for larger or more complex datasets.

Gradient-based optimization. The closed-form **least-squares** costs $\mathcal{O}(Nl^2 + l^3 + NlC)$ from the covariance computation and matrix inversion. If solved through stochastic gradient descent, the cost is $\mathcal{O}(NlCt)$ with t epochs.

Empirical runtime. Table A.5 shows that `least-squares` is faster than `k-means` in practice, likely because it processes all data in a single closed-form step rather than iterating class-by-class. Nevertheless, it should be clarified again that `least-squares` represents the analytic, non-iterative optimum derived from gradient minimization and lacks sequential class handling – precisely where imprinting excels (e.g., in continual or edge-learning scenarios).

Table A.5: Average runtime in seconds for different GEN variants across all 48 tasks (see section 4). To ensure transparency, all timing measurements were obtained on identical hardware (8 vCPUs on Intel Xeon Gold 6438Y+ nodes (2 sockets, 64 physical cores/128 threads)). Cores were not pinned to processes, which may introduce minor variance; however, we observed less than 10% variation across seeds.

GEN variant	Runtime (s)
mean	0.0029
5-means	1.2249
20-means	1.7321
least-squares	0.1593
5-least-squares	1.3724
20-least-squares	2.3717